LETTERS

Attosecond spectroscopy in condensed matter

A. L. Cavalieri[1], N. Müller[2], Th. Uphues[1,2], V. S. Yakovlev[3], A. Baltuška[1,4], B. Horvath[1], B. Schmidt[5], L. Blümel[5], R. Holzwarth[5], S. Hendel[2], M. Drescher[6], U. Kleineberg[3], P. M. Echenique[7], R. Kienberger[1], F. Krausz[1,3] & U. Heinzmann[2]

Comprehensive knowledge of the dynamic behaviour of electrons in condensed-matter systems is pertinent to the development of many modern technologies, such as semiconductor and molecular electronics, optoelectronics, information processing and photovoltaics. Yet it remains challenging to probe electronic processes, many of which take place in the attosecond (1 as = 10^{-18} s) regime. In contrast, atomic motion occurs on the femtosecond (1 fs = 10^{-15} s) timescale and has been mapped in solids in real time[1,2] using femtosecond X-ray sources[3]. Here we extend the attosecond techniques[4,5] previously used to study isolated atoms in the gas phase to observe electron motion in condensed-matter systems and on surfaces in real time. We demonstrate our ability to obtain direct time-domain access to charge dynamics with attosecond resolution by probing photoelectron emission from single-crystal tungsten. Our data reveal a delay of approximately 100 attoseconds between the emission of photoelectrons that originate from localized core states of the metal, and those that are freed from delocalized conduction-band states. These results illustrate that attosecond metrology constitutes a powerful tool for exploring not only gas-phase systems, but also fundamental electronic processes occurring on the attosecond timescale in condensed-matter systems and on surfaces.

Photoemission spectroscopy is based on the photoelectric effect, first explained by Einstein more than 100 years ago[6]. According to Einstein's law, photoelectrons ejected from a metal surface by light will have a kinetic energy that depends on the incident photon energy and the electron's original bound state energy. Photoelectron spectra will thus provide information about the electronic structure of the metal if well-characterized light sources are used[7]. Indeed, experiments using a broad range of photon energies have now been performed to determine the steady-state electronic properties of many bulk materials, thin films, and surfaces. The photoemission process itself involves three steps: excitation, transport, and ultimately escape of the photoelectron through the surface[8]. Here, in a proof-of-principle experiment, we combine this spectroscopy with attosecond temporal resolution to obtain time-domain insight into the electron transport stage of the photoemission process. The measurements represent (to our knowledge) the first direct attosecond time-resolved observation of electron transport in a condensed-matter system, and we expect that they will trigger other experimental research into the dynamics of processes that have attracted interest in solid-state and surface science. Such processes include charge transfer[9,10], charge screening[11], image charge creation and decay[12], electron–electron scattering[13], and collective electronic motion[14].

Time-resolved photoemission spectroscopy was originally implemented in the picosecond (1 ps = 10^{-12} s) to femtosecond regime, using first visible[15–17] and then extreme ultraviolet (XUV)[18,19] radiation. These experiments utilize one light pulse to trigger the dynamics, followed by a second light pulse to induce photoemission and thereby probe the transient state. Experiments using the laser-assisted photoelectric effect have been carried out[20–22]; but the XUV photoemission lasted over several wave cycles of the coincident near-infrared (NIR) light, limiting the time resolution to >10 fs. To overcome this limitation, we use single sub-femtosecond XUV pulses[4,5] for pumping, and coincident NIR waveform-controlled few-cycle laser pulses[23] as a probe[5]. The XUV pulse triggers the photoemission process, with only those photoelectron wave packets initiated from the uppermost atomic layers escaping without inelastic collision.
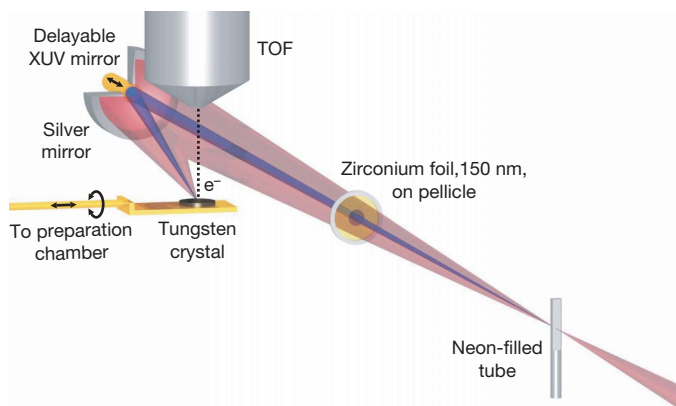

Figure 1 | Experimental set-up. Waveform-controlled, ~5-fs, 750-nm, 400-μJ laser pulses are focused with a mirror of 500-mm focal length into a ~2-mm-diameter tube filled with neon to generate XUV radiation by high-harmonic generation. The collinear XUV and NIR beams co-propagate towards a cored two-part mirror in the measurement chamber that is maintained under ultrahigh vacuum in a 1-m-length differential vacuum pumping stage, until the beams are separated by a pellicle/zirconium foil assembly. The zirconium foil transmits the XUV but blocks the NIR. The XUV radiation, indicated by the blue beam, is incident on a 6 eV (full-width at half-maximum FWHM) broad multilayer band-pass reflector centred at ~91 eV, which is mounted on a piezo-electric delay stage. With a proper XUV spectrum, the multilayer mirror reflects and focuses ~300-as (FWHM) XUV pulses. The NIR pulse, indicated by the violet beam, is reflected by a stationary (silver) outer annular mirror confocal with the inner mirror (f = 12.5 cm). Both pulses are focused onto the (110) surface of a tungsten single crystal that is mounted on a manipulator to control the angle of incidence. The manipulator is also used to retract the crystal into a preparatory chamber for cleaning. Resultant XUV-induced photoemission, which is detected by the time-of-flight spectrometer (TOF), is streaked by the coincident NIR laser pulse.

[1]Max-Planck-Institut für Quantenoptik, Hans-Kopfermann-Str. 1, D-85748 Garching, Germany. [2]Fakultät für Physik, Universität Bielefeld, D-33615 Bielefeld, Germany. [3]Department für Physik, Ludwig-Maximilians-Universität, Am Coulombwall 1, D-85748 Garching, Germany. [4]Institut für Photonik, Technische Universität Wien, Gußhausstr. 27, A-1040 Wien, Austria. [5]Menlo Systems GmbH, Am Klopferspitz 19, D-82152 Martinsried, Germany. [6]Institut für Experimentalphysik, Universität Hamburg, Luruper Chaussee 149, D-22761 Hamburg, Germany. [7]Dpto. Fisica de Materiales UPV/EHU, Centro Mixto CSIC-UPV/EHU and Donostia International Physics Center (DPIC), Paseo Manual de Lardizabal 4, 20018 San Sebastian, Spain.

Photoexcited electron wave packets propagate through the material in upper conduction bands, ultimately leaving the surface with an average kinetic energy determined by the XUV photon energy, the initial binding energy, and the material work function. An attosecond transient recorder (ATR), previously developed and used in gas-phase experiments[5], is used to observe the emitted photoelectron wave packet. In this scheme, the photoelectron momentum is further influenced by the electric field of a coincident few-cycle NIR laser pulse, giving rise to a 'streaked' final momentum distribution[24,25].

An ATR spectrogram is compiled by measuring a series of streaked photoelectron spectra with a time-of-flight detector, recorded as a function of time delay between the XUV pump and NIR streaking field. Important characteristics of the emitted electron wave packets, including their duration and frequency sweep, or 'chirp', can be determined from the spectra[24,25]. If measured for two or more different types of electrons, the complete ATR spectrograms can also yield relative timing information about the arrival of the wave packets on the surface, because the streaking effect is negligible until the electrons emerge from the surface (see Methods). The resolution of the ATR depends on the duration of the XUV excitation, the gradient of the streaking NIR field, and the signal-to-noise ratio in the photoelectron spectra.

In comparison to experiments performed on isolated atoms, ATR measurements in condensed-matter systems are more complicated because the photoelectron wave packets can be released from energy bands containing many distinct states rather than from a single, isolated energy level. Unoccupied conduction-band states just above the Fermi energy (defined by the highest occupied energy level in the absence of thermal excitation) might become populated by single-photon absorption of the leading edge of the NIR probe field prior to XUV photoemission, which is an unwanted complication. In contrast to conduction-band states, the localized 4f core states of tungsten are deeply bound and fully populated. Therefore, these states are unsusceptible to this potential influence of the streaking field, and constitute an ideal test case for proof of the extension of attosecond metrology to solids.

As a further challenge, above-threshold ionization (ATI) by the streaking field can, in condensed matter, generate energetic photoelectrons, obscuring detection of XUV-induced photoelectrons. ATI is favoured by the low work function of metals (as compared to the relatively high ionization potential of isolated atoms), which limits the intensity of the applied streaking field to levels far below those that can be used in gas-phase experiments.

As indicated by the diagram of the experimental set-up in Fig. 1, streaked photoemission spectra from a tungsten (110) crystal surface were recorded by collecting electrons within a narrow cone aligned perpendicularly to the surface. The relative delay between the XUV pulse and the NIR waveform-controlled streaking field was varied in 300-as steps in a sequence chosen to minimize systematic error, with
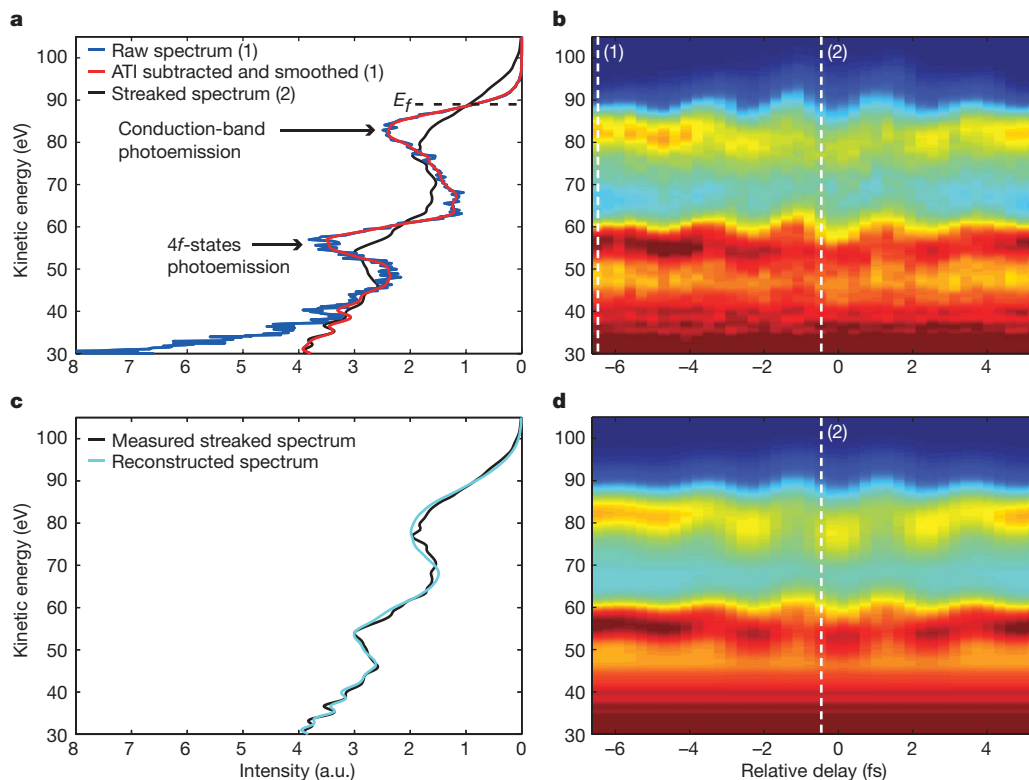

Figure 2 | Attosecond time-resolved photoemission spectra.
a, Photoelectron spectra collected at two different relative delays. The spectrum recorded at the delay indicated by the white dashed line labelled '(1)' in **b** is far from the zero of delay as defined by the overlap of the maximums of the NIR and XUV pulse envelopes. This spectrum shows pronounced peaks corresponding to the 4f-state and conduction-band photoemission. The blue line shows the raw spectrum as recorded by the time-of-flight detector, and the red line shows the corresponding spectrum after subtraction of NIR-induced ATI background and numerical smoothing. The 4f photoemission is peaked near 56 eV. The conduction-band photoemission is peaked near 83 eV, owing to a high density of d-band conducting states just below the Fermi energy. E_f denotes the kinetic energy of a photoelectron excited from the Fermi energy level. The other spectrum in **a** (displayed only after ATI subtraction and smoothing) was recorded near zero delay, as indicated by the white dashed line labelled '(2)'. At this delay,

the XUV pulse peak coincides with the NIR field maximum on our target. Consequently, the NIR vector potential crosses zero, giving rise to the strongest streaking and a clear broadening of the photoemission peaks is observed. **b,** The full ATI subtracted spectrogram for both the 4f-states and conduction-band photoemission. The streaking waveform (vector potential) is evident in both spectrograms, proving the extension of attosecond metrology to condensed-matter systems. We can expect that the energy modulation of the conduction-band peak should be a little larger than that of the 4f peak owing to their initial photoelectron kinetic energy. The amplitude of the spectral shift has a square-root dependence on initial kinetic energy (KE)[24], yielding an expected ratio in spectral shift of $\sqrt{KE_{cond}}/\sqrt{KE_{4f}} \approx 1.2$, which is consistent with our measurements. **c,** The reconstructed spectrum corresponding to that measured and displayed in **a**. **d,** The full simulated spectrogram.

spectra integrated for 60 s at each delay. (For a brief description of the experiment, see Methods Summary; full details regarding set-up, measurements and data analysis are provided as Supplementary Information.) Characteristic spectra obtained with our system are shown in Fig. 2a, indicating that emission from the conduction band occurs at a kinetic energy of ~83 eV while emission from the localized 4f states occurs at ~56 eV. At kinetic energies significantly below the 4f peak, the measured spectrum is due to NIR-induced ATI photoelectrons and XUV-generated photoelectrons that have undergone inelastic scattering.

The two distinct background components were distinguished by recording an additional photoelectron spectrum without the NIR streaking field. The ATI component was subsequently subtracted from the measured data (see Supplementary Information). This subtraction is illustrated for a fixed delay in Fig. 2a, and was performed at each of the delay steps, resulting in the full spectrogram presented in Fig. 2b. Here, a positive relative delay corresponds to the XUV pulse arriving earlier with respect to the streaking field at the surface. Both the 4f and conduction-band photoemission exhibit a pronounced periodic upshift and downshift in energy as a function of relative delay and, as in previous gas-phase experiments, the spectrogram reveals the waveform (vector potential) of the streaking field[5,26,27]. Our ability to resolve the field oscillation indicates that the photoemission from the 4f core states and from the conduction band is sub-femtosecond in duration, and proves that attosecond metrology has been successfully extended to condensed-matter systems.

Further examination reveals that the 4f spectrogram is shifted along the delay coordinate with respect to the conduction-band spectrogram. This effect is readily apparent upon inspection of the smoothed spectrograms that are obtained by interpolation of the measured data and shown in Fig. 3a. We quantify the temporal shift in the measured data by evaluating, for each delay step, the centre-of-mass (COM) of the spectral regions spanning the 4f and conduction-band peaks that cover the energy intervals 47–66 eV and 66–110 eV, respectively. Characterizing the periodic motion of the peaks through their COM requires no assumptions or fitting parameters, yet yields timing information that is invariant to fluctuations in the instantaneous laser parameters. The approach is also relatively insensitive to inelastic scattered background photoelectrons, which could not be subtracted from our measurements. As a result, the COM accurately describes the streaking-induced time-dependence of the energy shift of the 4f and conduction-band peaks, as shown in Fig. 3b.

By comparing the COM trajectories of the 4f and conduction band at the seven zero-crossings of the vector potential, we obtain seven independent measurements of their relative timing. This yields a temporal shift of $\Delta\tau = 110 \pm 70$ as between the ATR spectrograms of the conduction-band and 4f photoelectrons. (The error estimate results from a straightforward extrapolation of the error in calculating the COM; see Supplementary Information.) This shift or delay was observed in different independent measurements made at different locations on the tungsten sample, with the results corroborating the above value of $\Delta\tau$ to within the measurement error. We note that the rather large error associated with our $\Delta\tau$ value could be most effectively reduced in future measurements by using higher XUV photon energies and fluxes.

The shift between the two spectrograms indicates that, on average, photoelectrons originating from the localized 4f states emerge from the tungsten surface approximately 100 as later than those originating from the delocalized conduction band—even though the photoemission process for both types of electrons is initiated simultaneously by the same XUV pulse. The delay effect thus occurs during transport of the excited photoelectrons to the surface, illustrating that our technique provides a means to directly observe features of electron wave packet propagation towards the surface with attosecond precision.

By adapting a quantum mechanical model used in previous gas-phase streaking experiments[28], we are able to reconstruct the measured

spectra and spectrograms. The modelling of the streaking experiment requires some assumptions, leaving several parameters (such as duration of the electron wave packets, their chirp, and their emission time) for optimization. Figure 2c and d shows the reconstructions that best agree with experiment. These were obtained for wave packets with a duration of ~300 as (full-width at half-maximum, FWHM) and assuming a delay of ~100 as between the emission times of the electron wave packets, which supports the conclusions drawn from the COM analysis.

Our measurements also indicate that electron wave packets launched from both the localized 4f and delocalized conduction-band states are nearly undistorted on propagation to the surface. To explain the observed delay, we consider the group velocities for the two different photoelectron wave packets travelling in the solid. The crucial point is that after absorption of an XUV photon, the electron is excited into an upper conduction band region that depends on the electron's
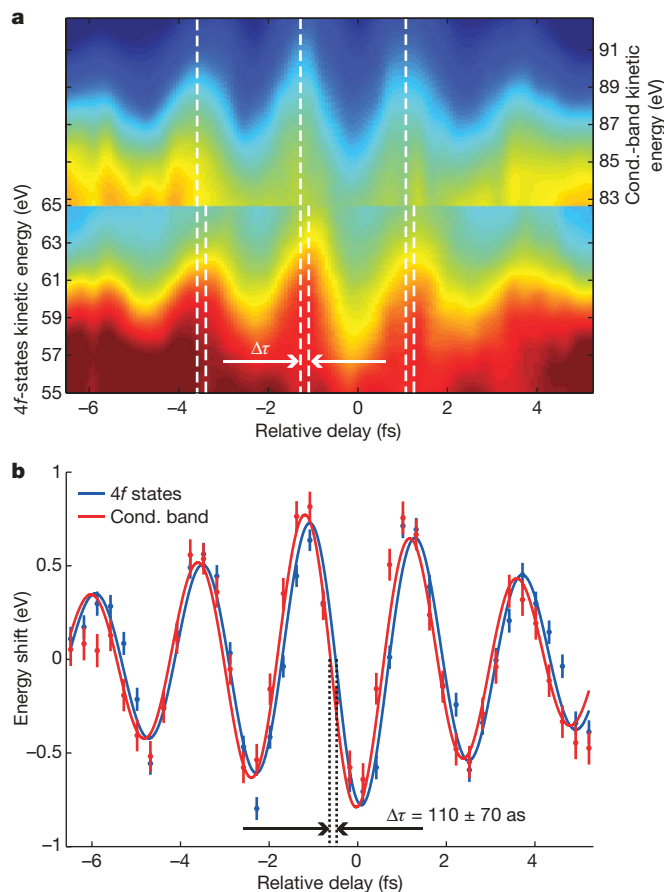

Figure 3 | Evidence of delayed photoemission. a, The 4f and conduction-band spectrograms, following cubic-spline interpolation of the measured data (but without background subtraction). The spectral region between ~65 eV and ~83 eV has been omitted to more easily compare the edges of the 4f and conduction-band peaks. A small shift in the relative delay is evident, as indicated by the white dashed lines through the fringes, and can be seen at each fringe maximum and minimum. Quantification of the shift of the 4f with respect to the conduction-band spectrogram is made by COM analysis, and is summarized in **b**. The energy intervals, within which the COMs were calculated, are 47–66 eV for the 4f photoemission peak and 66–110 eV for the conduction-band photoemission peak. Vertical error bars (±1 s.d.) are calculated from noise in the measured spectra (see Supplementary Information for details). For ease of visual comparison, the COM energy shift of the 4f spectral region was scaled by a factor of 2.5, to offset the stabilizing effect of the background plateau underneath the 4f peak (see Supplementary Information), in order to illuminate the ~100 as delay in emission. Rescaling these COM data points along the energy axis cannot influence the measured delay. The COM data points were fitted with a damped sinusoid, which corresponds to the NIR streaking field, to guide the eye.

initial binding energy and the XUV photon energy. If the relationship between momentum and energy of such an electron were that of a free electron, the ratio of velocities of the conduction-band and 4*f* electrons travelling with energies of 85 eV and 58 eV, respectively, would be a factor of ~1.2 (energy is defined with respect to the Fermi energy inside the material). However, elastic interactions with atoms in the crystal lattice, which give rise to electronic band structure, modify the momentum–energy relationship. This implies that in tungsten for XUV photon energies of ~91 eV, the mean velocity of the conduction-band photoelectrons is approximately twice that of the 4*f* photo-electrons (see Supplementary Information). We also note that due to their longer inelastic mean free paths[29], the slow 4*f* photoelectrons originate, on average, from ~1 Å deeper in the tungsten crystal than the fast conduction-band photoelectrons. On the basis of these considerations, we estimated the absolute delay between the initial excitation of a photoelectron and its escape through the surface to be ~60 as and ~150 as for the conduction and 4*f* photoelectrons, respectively. These values suggest a relative delay between photo-electron emissions from the surface of ~90 as, which is in good agreement with the observed delay in the emission of the 4*f* and conduction-band photoelectrons.

In summary, our observations demonstrate the successful extension of attosecond metrology to condensed-matter systems. Although the current experimental apparatus provides access to only the relative group delay in electron wave packet propagation, future measurements of absolute emission delays may be feasible using the same methods, for example by direct comparison with gas-phase ATR data. At this point, attosecond photoemission spectroscopy presents a clear path toward ultimately uncovering the intermediate processes leading to ejection of a photoelectron. This information might shed new light on data previously obtained with conventional time-integral photoemission spectroscopy and allow for accurate description of charge dynamics on the electronic timescale in both condensed matter and on surfaces.

METHODS SUMMARY

A 1-kHz-repetition-rate, waveform-controlled, few-cycle, ~5-fs, 400-μJ, 750-nm Ti:sapphire laser system is the front-end of our apparatus and is used in combination with proper spectral filtering to efficiently generate isolated attosecond pulses of XUV radiation by high-harmonic generation. As shown in Fig. 1, the XUV and NIR pulses co-propagate towards a two-part focusing mirror at near normal incidence. The inner component is a Mo/Si multilayer mirror and reflects the XUV radiation over a bandwidth of ~6 eV (FWHM) centred at ~91 eV, supporting 300-as transform-limited pulses[30]. The XUV mirror is mounted on a translation stage, providing a precise delay between the XUV pump and the NIR streaking pulse. The temporal resolution that can be achieved in pump-probe experiments using these pulses and this apparatus is expected to be a small fraction of the pulse half-width because XUV pulses generated with similar spectra and multilayer optics have previously been fully characterized and observed to be gaussian[24].

The tungsten surface must be sufficiently free of contamination to minimize photoelectron scattering on emission. Therefore, the measurement chamber is maintained under ultrahigh vacuum conditions with typical background pressures of $< 10^{-9}$ mbar, which suppresses the accumulation of contaminates on the crystal surface to a level permitting a full ATR spectrogram to be recorded without interruption.

In our application of the ATR, detection of electrons occurs in the direction normal to the tungsten crystal surface, and the NIR streaking field is incident on the tungsten (110) crystal surface near Brewster's angle (~75°). For this angle of incidence, owing to the refractive index of tungsten, photoelectron wave packets are not efficiently accelerated in the direction of observation until they emerge from the surface. Even though the streaking field penetrates the tungsten crystal, inside the material the electric field component along the surface normal is weaker by a factor of approximately 16, allowing us to neglect streaking effects until the electron wave packets emerge from the surface. The absence of effective streaking until the photoelectron emerges from the surface is generally the case for solids, allowing us to time processes occurring within the material.

Additional, detailed description of the experimental apparatus, measurement technique, and data analysis is provided in Supplementary Information.

1. Reis, D. A. & Lindenberg, A. M. in *Light Scattering in Solids IX* (eds Cardona, M. & Merlin, R.) 371–422 (Topics in Applied Physics 108, Springer, Berlin, 2007).
2. Fritz, D. M. *et al.* Ultrafast bond softening in bismuth: Mapping a solid's interatomic potential with X-rays. *Science* **315,** 633–636 (2007).
3. Pfeifer, T., Spielmann, C. & Gerber, G. Femto-second X-ray science. *Rep. Prog. Phys.* **69,** 443–505 (2006).
4. Hentschel, M. *et al.* Attosecond metrology. *Nature* **414,** 509–513 (2001).
5. Kienberger, R. *et al.* Atomic transient recorder. *Nature* **427,** 817–821 (2004).
6. Einstein, A. Über einen die Erzeugung und Verwandlung des Lichts betreffenden heuristischen Gesichtspunkt. *Ann. Phys.* **17,** 132–148 (1905).
7. Siegbahn, K. Electron-spectroscopy — outlook. *J. Electron Spectrosc. Relat. Phenom.* **5,** 3–97 (1974).
8. Berglund, C. N. & Spicer, W. E. Photoemission studies of copper and silver: theory. *Phys. Rev.* **136,** A1030–A1044 (1964).
9. Brühwiler, P. A., Karis, O. & Martensson, N. Charge-transfer dynamics studied using resonant core spectroscopies. *Rev. Mod. Phys.* **74,** 703–740 (2002).
10. Föhlisch, A. *et al.* Direct observation of electron dynamics in the attosecond domain. *Nature* **436,** 373–376 (2005).
11. Borisov, A., Sánchez-Portal, D., Díez-Muino, R. & Echenique, P. M. Dimensionality effects in time-dependent screening. *Chem. Phys. Lett.* **387,** 132–137 (2004).
12. Huber, R. *et al.* How many-particle interactions develop after ultrafast excitation of an electron-hole plasma. *Nature* **414,** 286–289 (2001).
13. Haight, R. Electron dynamics at surfaces. *Surf. Sci. Rep.* **21,** 277–325 (1995).
14. Cavalleri, A. *et al.* Tracking the motion of charges in a terahertz light field by femtosecond X-ray diffraction. *Nature* **442,** 664–666 (2006).
15. Yen, R. *et al.* Picosecond laser interaction with metallic zirconium. *Appl. Phys. Lett.* **40,** 185–187 (1982).
16. Höfer, U. *et al.* Time-resolved coherent photoelectron spectroscopy of quantized electronic states on metal surfaces. *Science* **277,** 1480–1482 (1997).
17. Petek, H. & Ogawa, S. Femtosecond time-resolved two-photon photoemission studies of electron dynamics in metals. *Prog. Surf. Sci.* **56,** 239–310 (1997).
18. Haight, R. & Peale, D. R. Tunable photoemission with harmonics of subpicosecond lasers. *Rev. Sci. Instrum.* **65,** 1853–1857 (1994).
19. Siffalovic, P. *et al.* Laser-based apparatus for extended ultraviolet femtosecond time-resolved photoemission spectroscopy. *Rev. Sci. Instrum.* **72,** 30–35 (2001).
20. Schins, J. M. *et al.* Observation of laser-assisted Auger decay in argon. *Phys. Rev. Lett.* **73,** 2180–2183 (1994).
21. Glover, T. E., Schoenlein, R. W., Chin, A. H. & Shank, C. V. Observation of laser assisted photoelectric effect and femtosecond high order harmonic radiation. *Phys. Rev. Lett.* **73,** 2180–2183 (1994).
22. Miaja-Avila, L. *et al.* Laser-assisted photoelectric effect from surfaces. *Phys. Rev. Lett.* **97,** 113604 (2006).
23. Baltuska, A. *et al.* Attosecond control of electronic processes by intense light fields. *Nature* **422,** 611–615 (2003).
24. Quéré, F., Mairesse, Y. & Itatani, J. Temporal characterization of attosecond XUV fields. *J. Mod. Opt.* **52,** 339–360 (2005).
25. Yakovlev, V., Bammer, F. & Scrinzi, A. Attosecond streaking measurements. *J. Mod. Opt.* **52,** 395–410 (2005).
26. Goulielmakis, E. *et al.* Direct measurement of light waves. *Science* **305,** 1267–1269 (2004).
27. Sansone, G. *et al.* Isolated single-cycle attosecond pulses. *Science* **314,** 443–446 (2006).
28. Kitzler, M., Milosevic, N., Scrinzi, A., Krausz, F. & Brabec, T. Quantum theory of attosecond XUV pulse measurement by laser dressed photoionization. *Phys. Rev. Lett.* **88,** 173904 (2002).
29. Tanuma, S., Powell, C. J. & Penn, D. R. Calculations of electron inelastic mean free paths. 2. Data for 27 elements over the 50–2000-eV range. *Surf. Interface Anal.* **17,** 911–926 (1991).
30. Wonisch, A. *et al.* Design, fabrication, and analysis of chirped multilayer mirrors for reflection of extreme-ultraviolet attosecond pulses. *Appl. Opt.* **45,** 4147–4156 (2006).